RSC Advances

PAPER

View Article Online
View Journal | View Issue

Cite this: *RSC Adv.*, 2022, **12**, 18093

A two-photon lysosome-targeted probe for endogenous formaldehyde in living cells†

Ting Cao *[a] and Hong Ma [b]

Received 27th April 2022
Accepted 6th June 2022

DOI: 10.1039/d2ra02672d

rsc.li/rsc-advances

Formaldehyde (FA) is a gaseous signaling molecule that plays a vital role in various biological processes as well as neurodegenerative diseases. Therefore, it is of great practical significance to develop effective and reliable chemical sensors for the monitoring of endogenous FA. Here, we designed and synthesized a two-photon (810 nm) turn-on chemosensor ***AMNT*** (aminomorpholine naphthalimide) that accurately localizes lysosomes in cells for imaging of cellular endogenous FA. The fluorescence emission peak of ***AMNT*** was at ~540 nm, with a slight blue shift (~528 nm) in response to FA, while the green fluorescence intensity increased. The probe exhibits excellent selectivity for FA among other biological interference species and a fast response time for FA. It is worth mentioning that the probe successfully imaged endogenous FA in cells in two-photon mode, making the probe an effective research tool in the biomedical field to study diseases related to abnormal FA expression.

1. Introduction

Formaldehyde (FA) is the simplest aldehyde among all aldehydes. According to the known literature,[1] FA is a human toxin and carcinogenic substance, which mainly comes from biomass combustion, solar humus degradation, vegetation and microbial decomposition, and gas emissions in industrial production.[2] FA plays an integral role in many applications due to its activity in reactive carbonyl species. For example, FA is effective in cross-linking with DNA and protein by forming stable methylene bridges; it is commonly used in cell immobilization and tissue preservatives.[3,4] The 35–40% FA aqueous solution is commonly called formalin, which can react with the amino groups on the proteins of organisms (including bacteria) and thus have antiseptic and bactericidal properties and can be used to soak biological specimens and so on. Nevertheless, the abuse of FA and the improper handling of industrial production have caused great harm to the natural environment of people's daily life and human health. Mainly reflected in these aspects, first of all, because of its strong carcinogenicity and reproductive toxicity,[5,6] FA is a genotoxic substance which can cause genetic mutations and lead to memory loss and neurological diseases.[7,8] Secondly, toxicological data indicate that the main hazard of FA is the expression of stimulation and sensitization. When FA reaches a certain concentration indoors, it can cause a major threat to human health through inhalation or ingestion, result in a variety of physical illness including heart disease, Alzheimer's, cancer and so on.[4,8–11] In the human body, endogenous FA originates from the methylation enzyme and oxidase mechanism and metabolism to regulate epigenetic generation, producing and maintaining normal endogenous by enzyme pathway within the range of 200–400 μM.[12–15] When FA is within the normal range of human body, it can expedite cellular proliferation and regulate the formation of memory.[16] However, once the content of FA in the human body over that concentration, because of the mechanism by which DNA binds to proteins lead to cognitive impairment in the body, it will lead to memory decline and neurodegenerative decay.[7,11,16]

It has important practical research significance for the analysis and monitoring of formaldehyde. According to literature surveys, a variety of methods have been developed to measure FA, including colorimetric assays,[17] HPLC/GC analysis,[18] radiometric assays,[19] and mass spectrometry[20] among others.[21] These techniques are limited in detection due to cumbersome sample processing operations, poor discrimination ability, low accuracy, lack of sensitivity, and the need to invasively destroy biological tissues. Therefore, a new monitoring method needs to be developed to overcome these problems.[22–24] With the progress and development of spectroscopic technology, fluorescence detection technology has become the most attractive small molecule detection technology.[25–28] Because of its high sensitivity, high selectivity, and good biocompatibility between cells and organisms, fluorescence imaging technology is used to analyse the effective tracking and monitoring method for analyzing specific substances in organisms.

By reviewing the literature, we found that FA production was associated with many organelles, including lysosomes,

[a]*Key Laboratory of Magnetic Molecules & Magnetic Information Materials Ministry of Education, The School of Chemical and Material Science, Shanxi Normal University, Taiyuan 030031, P. R. China. E-mail: caoting@sxnu.edu.cn; Fax: +86-931-8912582*

[b]*Department of Chemistry, Taiyuan Normal University, Jinzhong 030619, P. R. China*

† Electronic supplementary information (ESI) available. See https://doi.org/10.1039/d2ra02672d

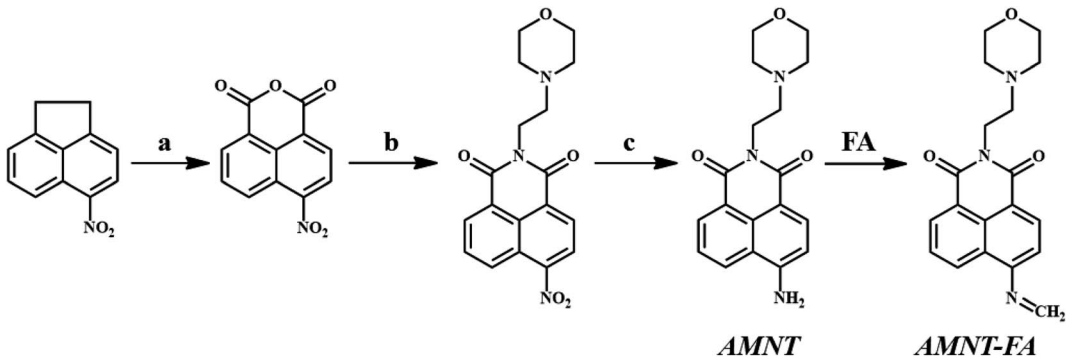

Scheme 1 The synthesis route of AMNT. (a) Potassium dichromate, CH_3COOH, reflux 10 h, Na_2CO_3 (neutralized pH = 7), 92%; (b) aminoethyl morpholine, EtOH, reflux 3 h, 86%; (c) $SnCl_2$, EtOH, reflux 4 h, Na_2CO_3 (neutralized pH = 7), 63%.

endoplasmic reticulum and Golgi apparatus.[10,12,24,29–32] Lysosomes are involved in cellular degradation, autophagy, the production of FA and other fundamental processes. Probes which can monitor localized FA in lysosomes received extensive attention from researchers. At the same time, abnormally high levels of endogenous FA can lead to various diseases, such as cancer, neurodegenerative diseases, diabetes, and chronic diseases of the liver and heart. Therefore, research on the detection and imaging of endogenous FA in living systems and organelles is of great significance in the biomedical field.

To date, few literature reports have reported lysosomal-targeted probes for monitoring endogenous FA.[29,30,33,34] Compared with the common single photon imaging, two-photon imaging has significant superiority.[35–37] For example, the near-infrared light at long wavelength has less cytotoxicity than short wavelength light, long wavelength light is less affected by scattering than short wavelength light and strong ability of tissue penetration. This is more conducive to image biomolecules in cells. In view of above advantages, we developed and synthesized ***AMNT***, a two-photon chemosensor in which naphthalimide acts as a precursor to locate the lysosomal FA *in vivo* (Scheme 1).

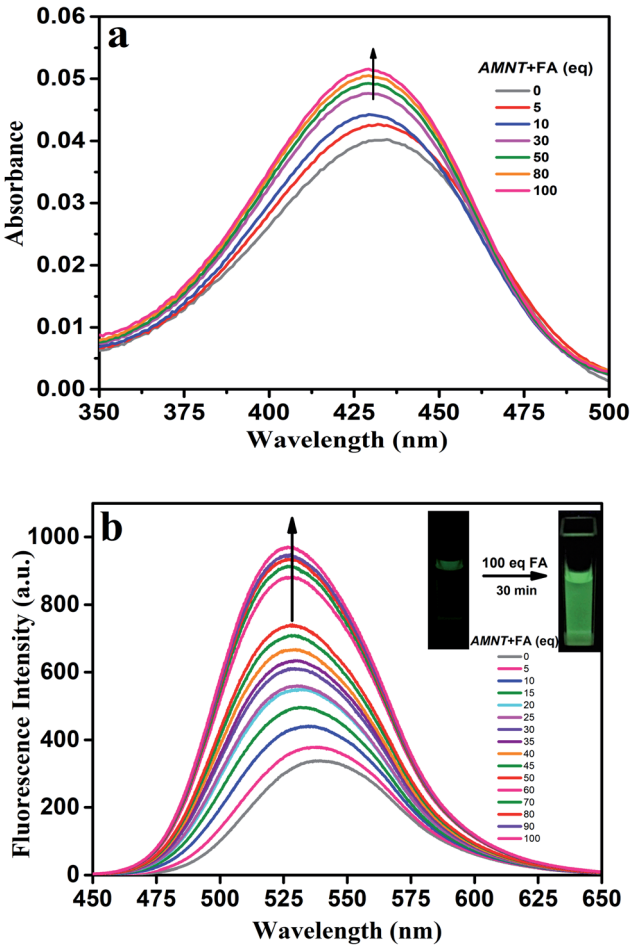

Fig. 1 (a) UV-vis absorption spectra of ***AMNT*** (10 μM) with different eq. of FA; (b) the emission spectra of ***AMNT*** (10 μM) reacted with different eq. of FA, λ_{ex} = 435 nm. Inset: fluorescence photo of ***AMNT*** (10 μM) under 365 nm UV lamp after reaction with 100 eq. FA.

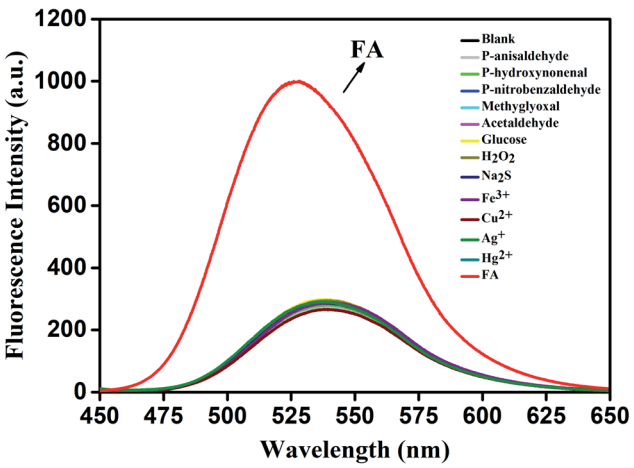

Fig. 2 Specific selectivity of ***AMNT*** (10 μM) reacted with 1000 μM different kinds of species. All spectra were obtained after 0.5 h of incubation with different analytes. (0) Probe ***AMNT***, (1) *p*-anisaldehyde, (2) *p*-hydroxynonenal, (3) *p*-nitrobenzaldehyde, (4) methylglyoxal, (5) acetaldehyde, (6) glucose, (7) H_2O_2, (8) Na_2S, (9) Fe^{3+}, (10) Cu^{2+}, (11) Ag^+ (12) Hg^{2+}, (13) FA.

2. Experimental

2.1. Instruments and methods

The FA used in the experiment comes from 37–40% of formaldehyde solution. All experiments were proceeded in PBS ($MeCN/H_2O = 1:9$, v/v, pH 7.4, 20 mM). All pH measurements in the experiment were performed using a pH-PE20 numerical pH device at room temperature.

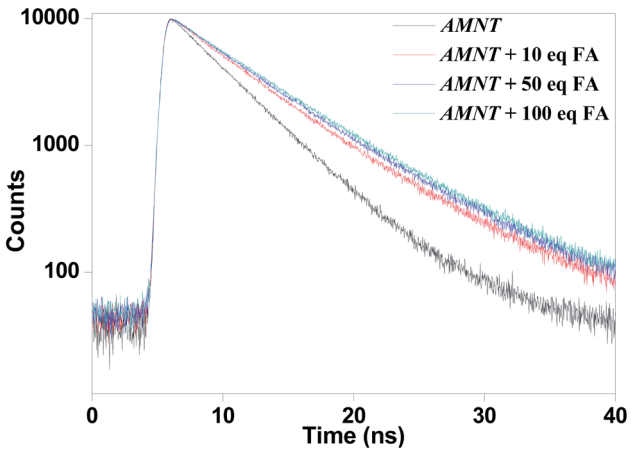

Fig. 3 Typical fluorescence attenuation curve for *AMNT* (10 μM).

2.2. Synthetic scheme of *AMNT*

A. Synthesis of 4-nitronaphthalic anhydride.[38] In a 100 ml round bottom flask, 3.73 g (20 mM) of potassium dichromate was dissolved in 20 ml of acetic acid, and then 1.01 g (5 mM) 4-nitroacenaphthene was dissolved in 10 ml of acetic acid and added dropwise into the above solution; after reflux of 10 h, the reaction mixture was cooled and filtered into ice water. The remaining residue was washed to neutral with Na_2CO_3, and dried to obtain yellow compound 1 for the next experiment (1.12 g) with 92% yield.

B. Synthesis of morpholino-4-nitronaphthalic anhydride.[39] The above product 0.36 g (1.5 mmol) was dissolved in 10 ml ethanol, and then 1.75 ml (4.5 mmol) aminoethyl morpholine was added and the mixture was heated to reflux for 3 h, cooled to room temperature, filtered, washed with ethanol, the filtrate was evaporated to obtain yellow solid compound 2 (0.452 g) with 86% yield.

C. Synthesis of morpholino-4-aminonaphthalic anhydride (*AMNT*). 0.355 g (1 mmol) of the above product was dispersed in ethanol, $SnCl_2$ (0.569 g, 3 mmol) was dissolved in 2 ml of concentrated HCl, and it was added dropwise to the reaction system, and the reactant heating and reflux 4 h. After reaction completed, cooled down, then neutralized with Na_2CO_3, filtered with suction, washed with distilled water, extracted with $CHCl_2$ and the solvent removed under reduced pressure and then fractionated by silica gel flash chromatography isolation ($CHCl_2/MeOH = 10:1$) to give compound ***AMNT*** as a yellow solid (0.205 mg) in 63% yield.

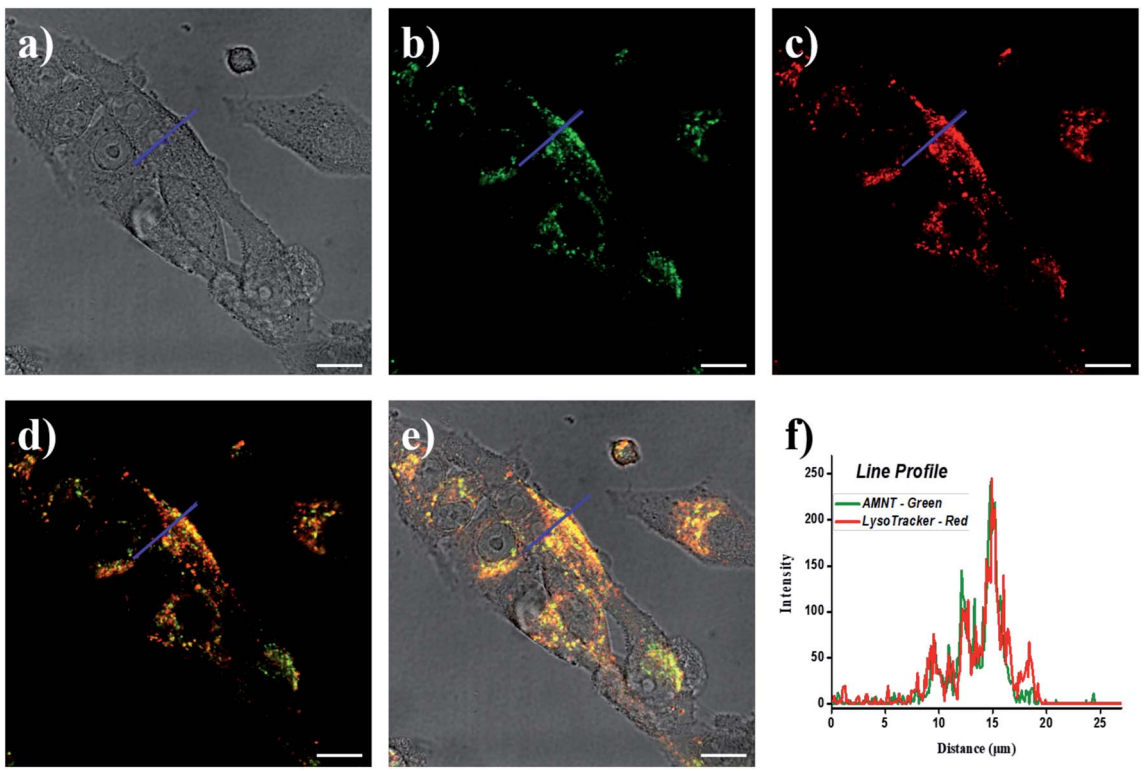

Fig. 4 Lysosome-targeting imaging of HeLa cells: (a) the bright field; (b) the green channel of *AMNT*; (c) the red channel of LysoTracker; (d) the overlap field of (b) and (c); (e) the overlap field of (a), (b), (c); (f) the line profile of lysosome-targeting in cells. All cells were cultivate with 500 μM FA after incubated with *AMNT* (10 μM), $\lambda_{ex} = 458$ nm, scale bar = 7.5 μm.

3. Results and discussion

3.1. UV-vis absorption and emission spectra

After confirming and characterizing the structures of ***AMNT+FA*** (Fig. S13†) and ***AMNT*** (Fig. S11 and S12†), spectral experiments were carried out. The UV-absorption and emission photophysical data of ***AMNT*** response FA are listed in Table S1.† As shown in the absorption spectrum curve of Fig. 1a, the absorption band at 435 nm arised and the intensity enhanced with the increased concentration of FA. In Fig. 1b, ***AMNT*** has a maximum emission band at ~540 nm and a lower Φ_f (fluorescence quantum yield) is 0.115 ± 0.003. After upon addition of FA, the maximum peak of fluorescence emission blue-shift (~540 to ~528) and fluorescence intensity increases with the increase of FA concentration. The low Φ_f of the probe ***AMNT*** should be attributed to the ICT (intramolecular charge transfer) properties of the excited condition. When treated with FA, the Schiff base reaction can effectively quench ICT process of the amine moiety to naphthalimide unit by reducing the electron donating effect of the amine, thereby causing the increased Φ_f yield is 0.217 ± 0.012.

3.2. The selectivity of *AMNT* towards FA

In order to characterize the single selectivity of the probe ***AMNT*** in aqueous solution, various representative chemicals, such as aldehydes and other interfering substances, are measured in the PBS buffer. As shown in Fig. 2, it can be seen that the fluorescence intensity of the other substances to be detected did not change significantly except for FA. Under the same conditions, only the fluorescence intensity treated with FA increased significantly, which confirms that the probe ***AMNT*** has an excellent selectivity for FA (Fig. S3†).

3.3. Time-response, detection limit and the effect of pH

Fluorescence response curves of ***AMNT*** (10 μM) with different equiv. of FA is shown in Fig. S1.† In fact, the known response time to monitor FA is generally from 1–4 h. It is worth noting that ***AMNT*** within 10–200 equiv. FA reaction progress curve rises sharply in 10 min, and then in the 30 min are basically stable to achieve the relative maximum which shows favorable response of ***AMNT*** towards FA. It is good to be glad that the reaction time is faster than most of the known literature[10,12,24,29,30,34,40–46] (Table S3†). In addition, ***AMNT*** also shows good light stability (Fig. S5†).

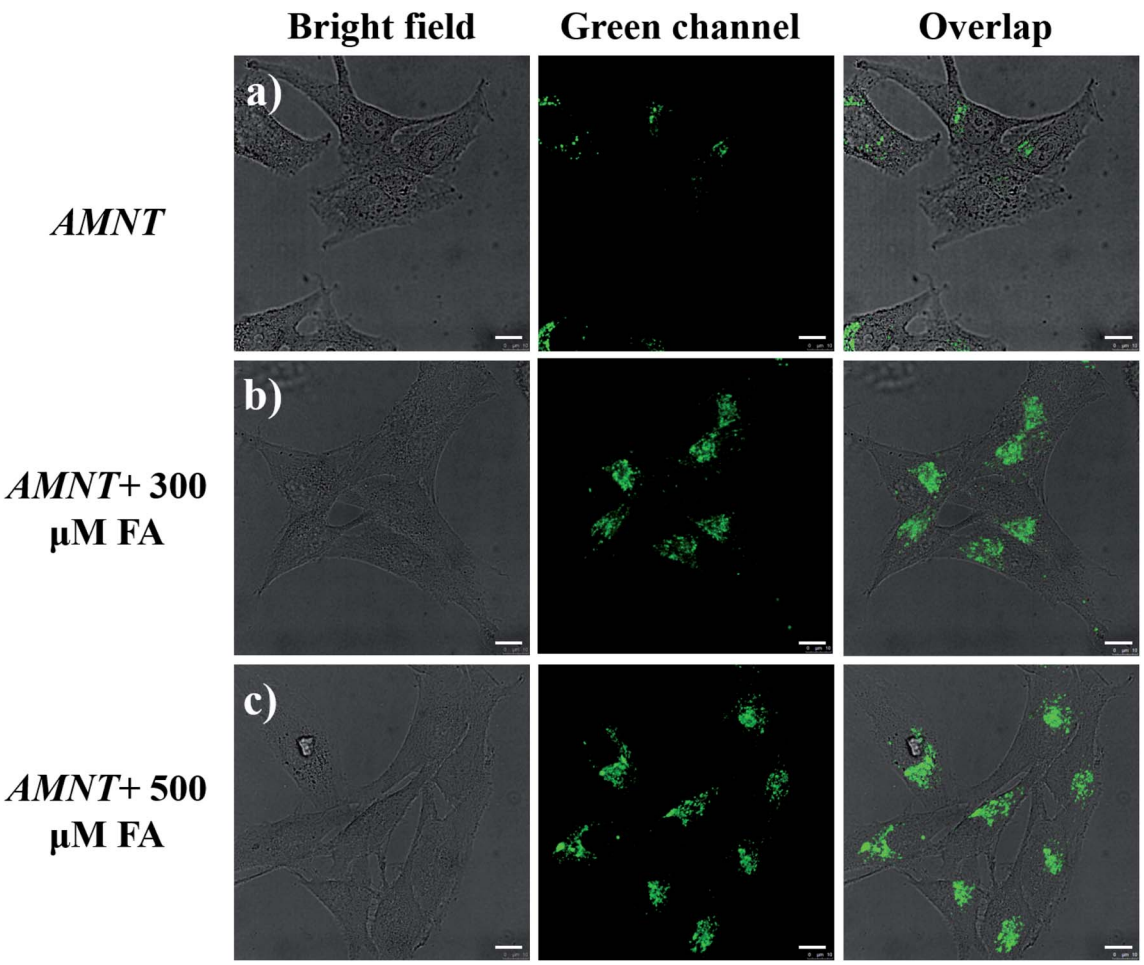

Fig. 5 Confocal imaging of HeLa cells: (a) the first row as a control was incubated with ***AMNT***; (b) the second to (c) the third row are images after adding 300/500 μM FA to ***AMNT*** (10 μM), respectively, $\lambda_{ex} = 458$ nm, green channel: 510–550 nm, scale bar = 10 μm.

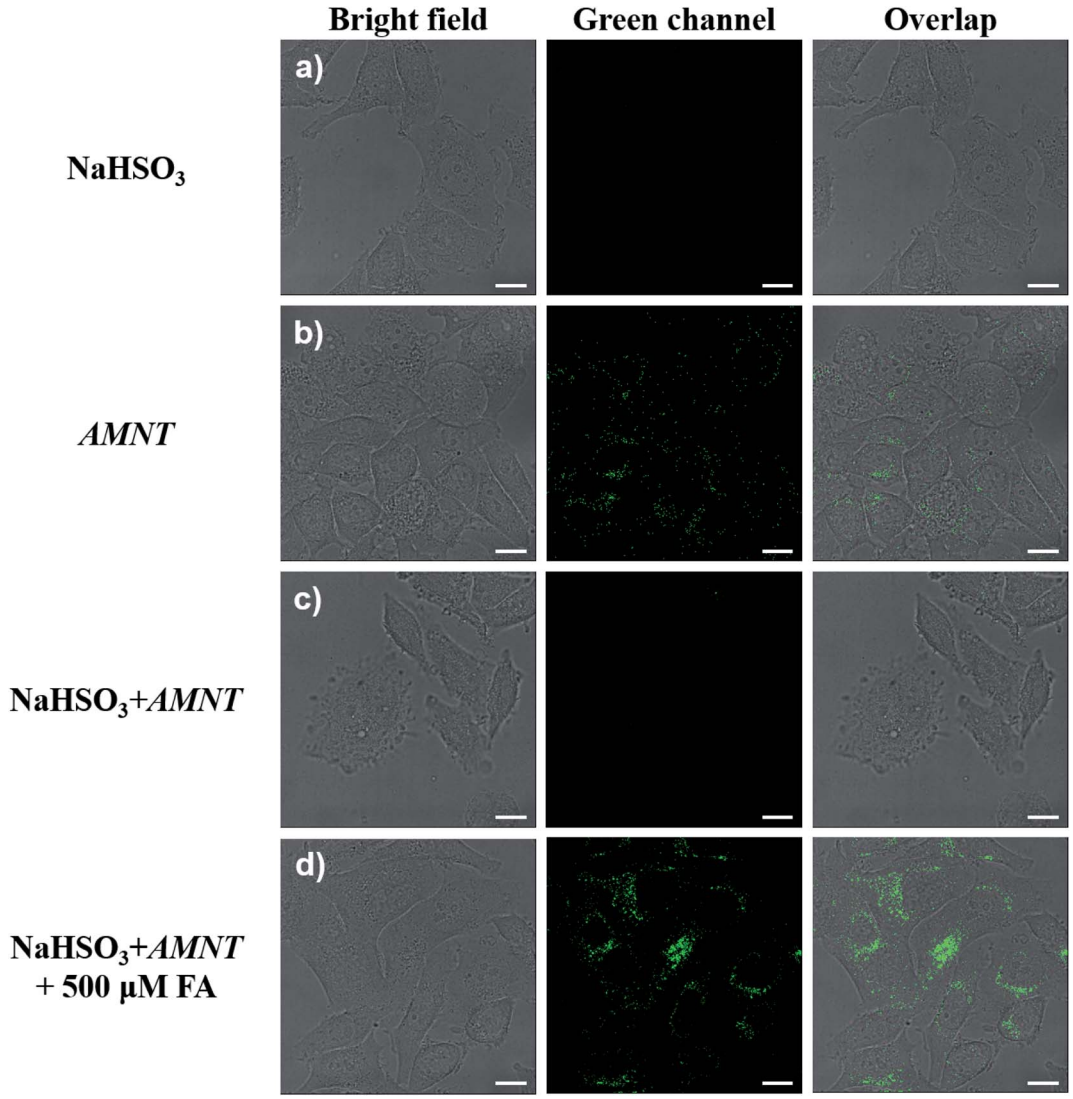

Fig. 6 The cell imaging of spontaneous FA, (a) the $NaHSO_3$ inhibitor pretreatment group; (b) control group with only probes; (c) the experimental group in which the inhibitor was pretreated first, and then the probe was added; (d) the experimental group in which the inhibitor was pretreated first, then the probe was added to incubate, and finally FA was added. ***AMNT*** = 10 μM, $NaHSO_3$ = 200 μM, λ_{ex} = 458 nm, green channel: 510–580 nm, scale bar = 10 μm.

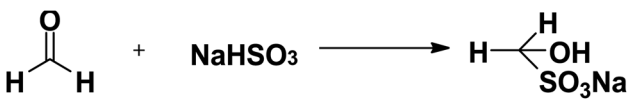

Scheme 2 The response mechanism of $NaHSO_3$ towards FA.

When the probe was treated with 0–500 μM FA, the fluorescence intensity increased linearly. The calibration curve is shown in Fig. S2,† and the detection limit is calculated to be 1.77 μM, which is lower than most reported references (Table S3†).

The ***AMNT*** shows a certain stable fluorescence intensity in pH 4–10 range. When FA is added, the fluorescence intensity is stable in the range of pH 6–10, and has a wide range of pH response (Fig. S4†).

3.4. Fluorescence life-time measurements of *AMNT* towards FA

The fluorescence decay curves of different concentrations of FA interacting with ***AMNT*** in PBS buffer were tracked using single-photon timing method. As shown in Fig. 3, the fluorescence decay curves of different concentrations of FA in response to ***AMNT*** in PBS buffer were tracked by single-photon timing. The test was performed after adding different equivalents of FA to the PBS solution containing 10 μM of ***AMNT*** for 30 min. For the blank sample with only ***AMNT***, the single-photon fluorescence decay curves were collected at excitation wavelength of 435 nm and emission wavelengths of 530, 540, and 550 nm, respectively. The samples in the analysis group added with FA were also excited at 435 nm, and their single-photon fluorescence decay curves were measured at emission wavelengths of 520, 530, and 540 nm, respectively. Generally, FAST software is used to global

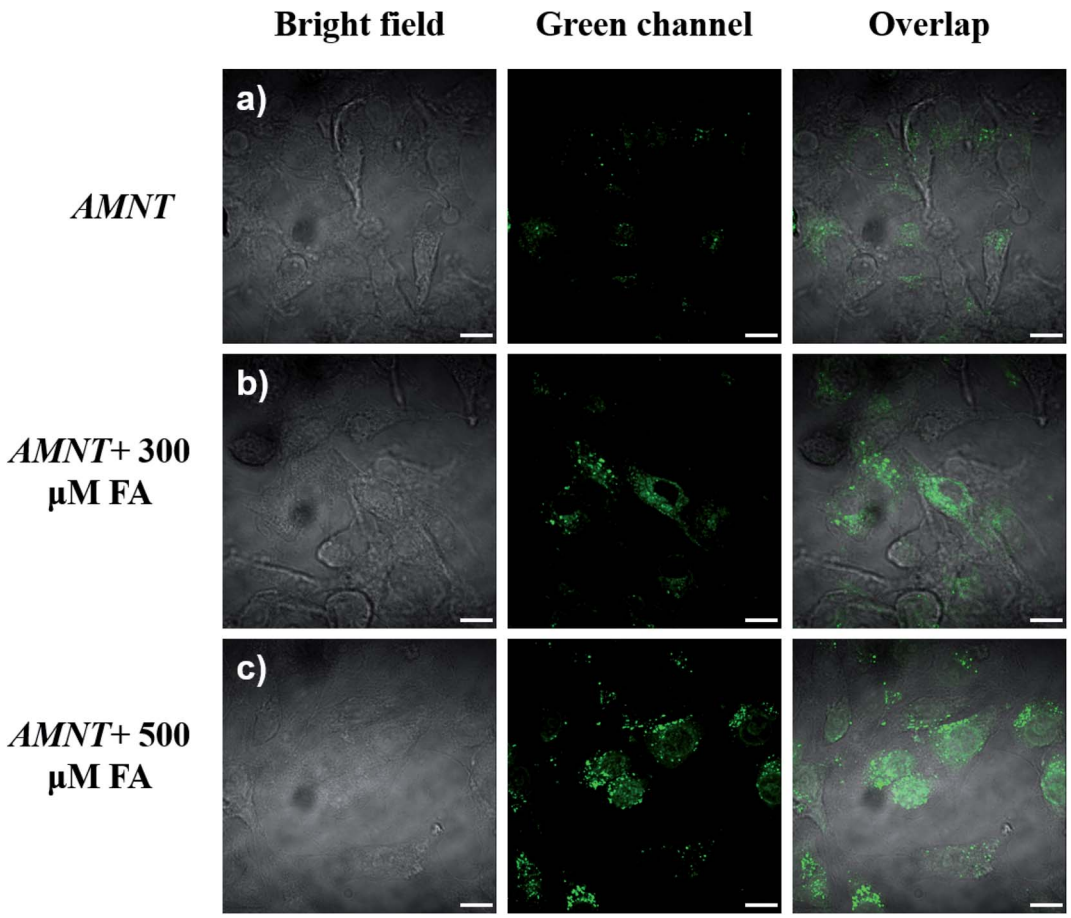

Fig. 7 Two-photon confocal fluorescence images of ***AMNT*** towards FA. (a) Control group with probe incubation; (b) the experimental group that added probe first and then added 300 μM FA; (c) the experimental group that added the probe first and then added 500 μM FA. ***AMNT*** = 10 μM, λ_{ex} = 810 nm, green channel: 510–550 nm, scale bar = 10 μm.

analysis the three decay trajectories of different emissions, and the decay time τ_i and pre-exponential factors α_i can be obtained with higher precision. The relevant fitted data are shown in Table S2 and Fig. S10.† From the data analysis, it can be seen that the fluorescence decay curve of ***AMNT*** fits two exponential functions, where τ_1 = ~4.13 is the main amplitude, which belongs to the fluorescence lifetime of the naphthalimide chromophore, and τ_2 = ~10.33 ns is attributable to the formation lifetime of a small number of aggregates (formed by the π, π-stacking effect). With the addition of FA and the increase of its concentration, the fluorescence decay also changed significantly. τ_1 remained almost constant (~4.6 ns) and the amplitude decreased with increasing FA concentration (95~32%). Meanwhile, the lifetime of τ_2 (10.3~7.6 ns) decreased with increasing amplitude (4~67%), this faster decay can be attributed to the products generated after the ICT process that occurs when the amino moiety of the naphthalimide fluorophore interacts with FA.

3.5. Lysosome-targeting ability of *AMNT* in living cell

Many known reports indicate that morpholine has the ability to target lysosomes in living cells. As a consequence, we carried out a co-localization experiment to study the lysosomal targeting ability of ***AMNT***. In order to better verify the lysosome-targeted effect of the probe, the commercially recognized lysosomal probe LysoTracker Red, a commonly used lysosome-targeted dye with red fluorescence, was used as a control for lysosome staining. As shown in Fig. 4, HeLa cells were cultivated with ***AMNT*** (10 μM) for 1 h and after that FA (500 μM) added in for 1 h and then stained further with commercial LysoTracker Red (10 μM) for another 30 min, under the excitation of 458 nm and 565 nm, the green channel (510–560 nm) and the red channel (580–630 nm) was found to be overlapped perfectly. The overlap coefficient was calculated as 0.93, indicates the good location of ***AMNT*** in lysosomes. The above experimental result shows that ***AMNT*** has high lysosomal specific targeting to FA.

3.6. The application of *AMNT* towards FA in cells imaging

In order to further determine the applicability of ***AMNT*** in cell imaging, the toxicity of FA and ***AMNT*** to HeLa cells was evaluated by cytotoxicity assay. From the data in Fig. 5a, low concentrations of FA had little effect on cells, while the viability of cells was slightly reduced at higher concentrations. The cell

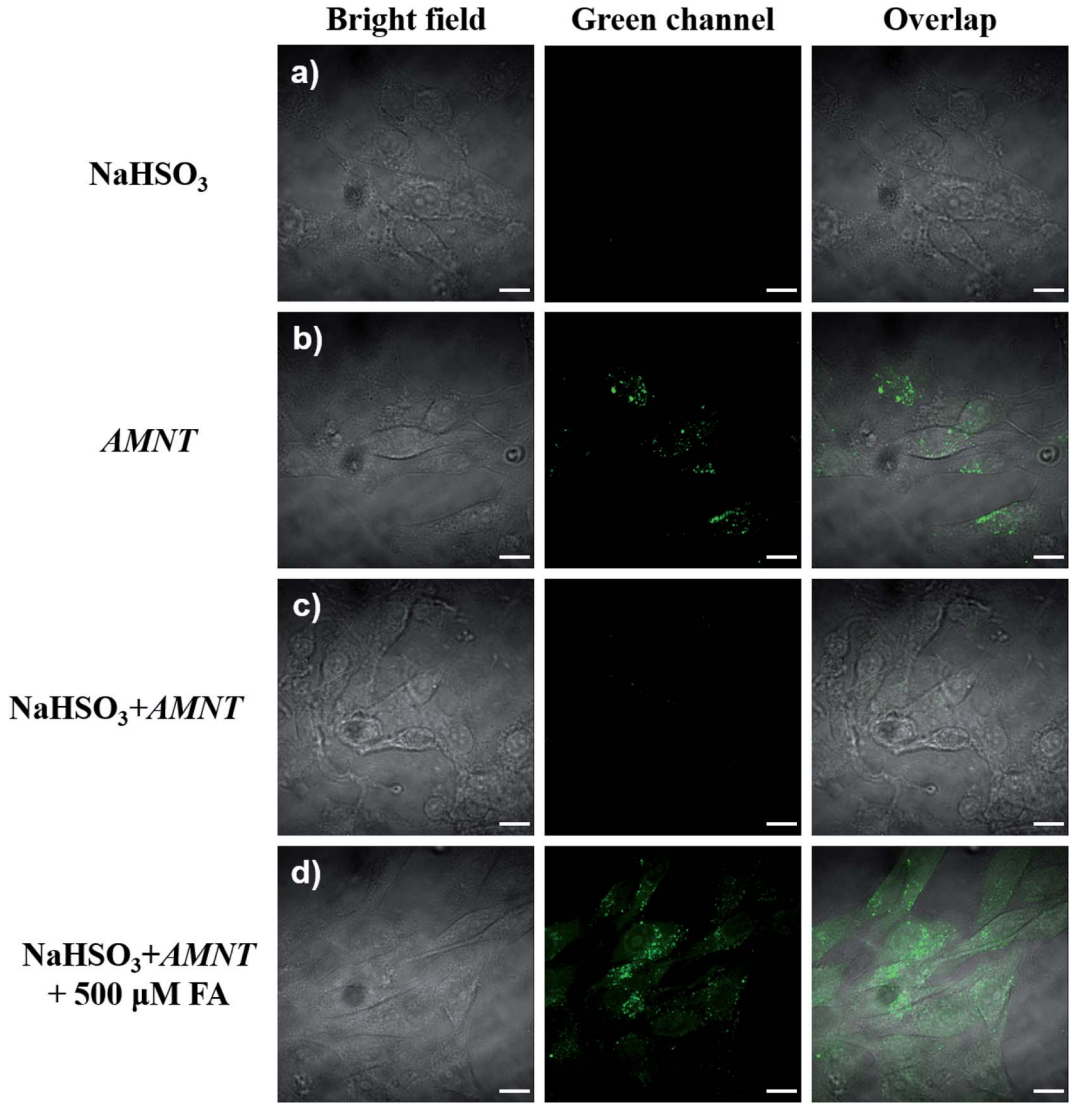

Fig. 8 Two-photon confocal fluorescence images of ***AMNT*** towards endogenous FA. (a) the $NaHSO_3$ inhibitor pretreatment group; (b) control group with only probes; (c) the experimental group in which the inhibitor was pretreated first, and then the probe was added; (d) the experimental group in which the inhibitor was pretreated first, then the probe was added to incubate, and finally FA was added. ***AMNT*** = 10 μM, $NaHSO_3$ = 200 μM, λ_{ex} = 810 nm, green channel: 510–550 nm, scale bar = 10 μm.

viability shown in Fig. 5b remained almost unchanged, indicating that ***AMNT*** have little cytotoxicity and good biocompatibility. These experimental phenomena suggest that this probe can be effectively applied to the imaging of FA in cells.

An experiment was performed to evaluate the cell imaging ability of the probe ***AMNT*** for FA. As a blank control group, it can be seen from Fig. 6a that the fluorescence of the green channel was weak after the HeLa cells were cultured for 1 h, Meanwhile, the other group cells of Fig. 6b and c were added with 300/500 μM FA incubated for 0.5 h after being treated with the probe ***AMNT*** for 1 h. The cells images clearly showed strong green fluorescence in green channel, and the greater the FA concentration, the stronger the fluorescence intensity. Due to the probe is designed and synthesized as small organic molecule, the size is suitable for transmembrane transport. After a period of incubation, it can easily enter the organelles from the cytoplasm. Morpholine based naphthalimide fluorescent probe is used to detect and image FA in lysosomes. The hydrazidetion reaction and FA mediated cleavage reaction depend on the acidic environment, making the probe easier to aggregate in lysosomes. Therefore, the probe mainly reacts with formaldehyde in lysosome.[29,30,34] These results indicate that ***AMNT*** is able to be used for detecting the content of FA in living cells successfully and specifically recognize FA in lysosomes.

Next, we further tried the feasibility of ***AMNT*** for imaging endogenous FA in living cells. Sodium hydrogen sulfite ($NaHSO_3$) is used as an available and not complicated FA inhibitor.[10,29] Owing to the reaction can effectively happened among HSO_3^- with FA by destroy the carbonyl group of FA (Scheme 2). To confirm the suitability of inhibitor, we determined the spectral curve in Fig. S6.† The spectral curve of Fig. S6† shows that the fluorescence of the probe ***AMNT*** treated

with HSO_3^- is almost unchanged, and the fluorescence is enhanced after the addition of FA. However, after the addition of HSO_3^- in advance, the fluorescence intensity of the FA sample to which the probe ***AMNT*** was added hardly changed (Fig. S7†). By analyzing these data, $NaHSO_3$ is indeed a potent inhibitor of FA.

Imaging was performed using a laser confocal microscope, and no fluorescence was appeared in the green channel of HeLa cells cultured with HSO_3^- after 0.5 h. HeLa cells after cultured with the probe ***AMNT*** for 1 h showed stronger green fluorescence (Fig. 6b), while the cells pretreated with the inhibitor HSO_3^- for 0.5 h and co-incubated with the probe ***AMNT*** for 1 h had almost no green fluorescence (Fig. 6c). It indicated that the inhibitor HSO_3^- effectively inhibited the reaction between endogenously produced FA and ***AMNT***. Meanwhile, in order to further confirm that the phenomenon of fluorescence enhancement is indeed caused by the interaction between FA and ***AMNT***, we continued to add FA exogenously to this group of cells. Due to HSO_3^- is quantitative and does not react with ***AMNT***, bright green fluorescence can be observed from the imaging image of ***AMNT*** in cells after the addition of exogenous FA (Fig. 6d). This is also consistent with the experimental phenomenon reported in the literature.[10]

3.7. Two-photon properties and application in cells imaging

It's known that naphthalimide fluorophore have the mature two-photon property.[10,29,40] We measured the fluorescence integral area and two-photon absorption (TPA) cross section of ***AMNT*** (Fig. S8†) *via* two-photon excitation. The data show that the integral area of ***AMNT*** reaches the maximum value at 850 nm, and the absorption cross section at 800 nm is the largest (~80 GM). Under the same test conditions, the integral area of ***AMNT-FA*** in 800 nm reaches the maximum and the absorption cross section at 850 nm is the largest (~66 GM). On this basis, two-photon fluorescence confocal microscopy was used to evaluate the imaging of probe ***AMNT*** in HeLa cells. 10 μM of ***AMNT*** was cultured with HeLa cells for 1 h, followed by addition of FA (300/500 μM) for 1 h, and then HeLa cells were imaged with an excitation wavelength of 810 nm. As shown in Fig. 7a, cells showed weaker green fluorescence in the presence of only the probe ***AMNT***, and in comparison, cells cultured with 300/500 μM FA (Fig. 7b and c) showed significant green fluorescence. The experimental results confirmed that the probe ***AMNT*** can be used for FA two-photon imaging detection in living cells.

At the same time, we also carried out two-photon imaging experiment on endogenous FA. As shown in Fig. 8a, under the excitation of 810 nm, only in the presence of $NaHSO_3$, the green channel has no fluorescence. However, in Fig. 8b, only in the presence of the probe ***AMNT***, cells showed the stronger green fluorescence. In Fig. 8c, the probe ***AMNT*** shows no fluorescence in the cells pretreated with the inhibitor $NaHSO_3$, after the probe ***AMNT*** and FA were further added to the cells previously treated with the $NaHSO_3$ inhibitor, strong green fluorescence was observed. These results indicate that ***AMNT*** is an excellent probe for two-photon imaging of intracellular FA.

4. Conclusions

In summary, a novel water-soluble, highly selective, fast response time and lower detection limit turn-on two-photon lysosome-targeted probe of FA has been rationally designed and synthesized. The probe ***AMNT*** is a naphthalimide-derived and the occurrence of Schiff based reaction between ***AMNT*** and FA is based on the ICT reduction process. It is worth mentioning that the results of this work indicates that ***AMNT*** can track endogenous FA in living cells in the mode of two-photon imaging. It is possible to realize the further application of the probe in the research field of FA related diseases.

Conflicts of interest

There are no conflicts to declare.

References

1 R. G. Liteplo, R. Beauchamp, M. E. Meek, R. Chenier, *Formaldehyde (Concise International Chemical Assessment Documents)*, World Health Organization, Geneva, 2002.
2 T. F. Brewer and C. J. Chang, *J. Am. Chem. Soc.*, 2015, **137**, 10886–10889.
3 A. Songur, O. A. Ozen and M. Sarsilmaz, in *Reviews of Environmental Contamination and Toxicology*, Springer, 2010, pp. 105–118.
4 K. Tulpule and R. Dringen, *J. Neurochem.*, 2013, **127**, 7–21.
5 L. Gu, Y. Tang and W. Lin, *Tetrahedron*, 2021, **78**, 131808.
6 Z. Tong, W. Luo, Y. Wang, F. Yang, Y. Han, H. Li, H. Luo, B. Duan, T. Xu, Q. Maoying, H. Tan, J. Wang, H. Zhao, F. Liu and Y. Wan, *PLoS One*, 2010, **5**, e10234.
7 M. Unzeta, M. Sole, M. Boada and M. Hernandez, *J. Neural Transm.*, 2007, **114**, 857–862.
8 M. Hauptmann, P. A. Stewart, J. H. Lubin, L. E. Beane Freeman, R. W. Hornung, R. F. Herrick, R. N. Hoover, J. F. Fraumeni Jr, A. Blair and R. B. Hayes, *J. Natl. Cancer Inst.*, 2009, **101**, 1696–1708.
9 M. Hauptmann, P. A. Stewart, J. H. Lubin, L. E. Beane Freeman, R. W. Hornung, R. F. Herrick, R. N. Hoover, J. F. Fraumeni Jr, A. Blair and R. B. Hayes, *JNCI, J. Natl. Cancer Inst.*, 2009, **101**, 1696–1708.
10 Y. Tang, X. Kong, A. Xu, B. Dong and W. Lin, *Angew. Chem., Int. Ed.*, 2016, **55**, 3356–3359.
11 Z. Tong, J. Zhang, W. Luo, W. Wang, F. Li, H. Li, H. Luo, J. Lu, J. Zhou, Y. Wan and R. He, *Neurobiol. Aging*, 2011, **32**, 31–41.
12 A. Roth, H. Li, C. Anorma and J. Chan, *J. Am. Chem. Soc.*, 2015, **137**, 10890–10893.
13 Y. Fu, G. Z. Luo, K. Chen, X. Deng, M. Yu, D. Han, Z. Hao, J. Liu, X. Lu, L. C. Dore, X. Weng, Q. Ji, L. Mets and C. He, *Cell*, 2015, **161**, 879–892.
14 E. L. Greer, M. A. Blanco, L. Gu, E. Sendinc, J. Liu, D. Aristizabal-Corrales, C. H. Hsu, L. Aravind, C. He and Y. Shi, *Cell*, 2015, **161**, 868–878.
15 G. Zhang, H. Huang, D. Liu, Y. Cheng, X. Liu, W. Zhang, R. Yin, D. Zhang, P. Zhang, J. Liu, C. Li, B. Liu, Y. Luo,

Y. Zhu, N. Zhang, S. He, C. He, H. Wang and D. Chen, *Cell*, 2015, **161**, 893–906.
16 Z. Q. Tong, C. S. Han, W. H. Luo, H. Li, H. J. Luo, M. Qiang, T. Su, B. B. Wu, Y. Liu, Y. Xu, Y. Wan, D. H. Cui and R. Q. He, *Sci. Rep.*, 2013, **3**, 1807.
17 T. Nash, *Biochem. J.*, 1953, **55**, 416.
18 U. Riess, U. Tegtbur, C. Fauck, F. Fuhrmann, D. Markewitz and T. Salthammer, *Anal. Chim. Acta*, 2010, **669**, 53–62.
19 T. Szarvas, E. Szatlóczky, J. Volford, L. Trézl, E. Tyihák and I. Rusznák, *J. Radioanal. Nucl. Chem.*, 1986, **106**, 357–367.
20 S. Kato, P. J. Burke, T. H. Koch and V. M. Bierbaum, *Anal. Chem.*, 2001, **73**, 2992–2997.
21 P. H. Yu, C. Cauglin, K. L. Wempe and D. Gubisne-Haberle, *Anal. Biochem.*, 2003, **318**, 285–290.
22 K. J. Bruemmer, O. Green, T. A. Su, D. Shabat and C. J. Chang, *Angew. Chem., Int. Ed. Engl.*, 2018, **57**, 7508–7512.
23 Y. Tang, Y. Zhao and W. Lin, *Nat. Protoc.*, 2020, **15**, 3499–3526.
24 T. F. Brewer and C. J. Chang, *J. Am. Chem. Soc.*, 2015, **137**, 10886–10889.
25 Q. Wan, S. Chen, W. Shi, L. Li and H. Ma, *Angew. Chem., Int. Ed. Engl.*, 2014, **53**, 10916–10920.
26 J. J. Hu, N. K. Wong, S. Ye, X. Chen, M. Y. Lu, A. Q. Zhao, Y. Guo, A. C. Ma, A. Y. Leung, J. Shen and D. Yang, *J. Am. Chem. Soc.*, 2015, **137**, 6837–6843.
27 X. Wu, M. Yu, B. Lin, H. Xing, J. Han and S. Han, *Chem. Sci.*, 2015, **6**, 798–803.
28 S. Bhuniya, S. Maiti, E. J. Kim, H. Lee, J. L. Sessler, K. S. Hong and J. S. Kim, *Angew. Chem., Int. Ed. Engl.*, 2014, **53**, 4469–4474.
29 Y. Tang, X. Kong, Z.-R. Liu, A. Xu and W. Lin, *Anal. Chem.*, 2016, **88**, 9359–9363.
30 X. Xie, F. Tang, X. Shangguan, S. Che, J. Niu, Y. Xiao, X. Wang and B. Tang, *Chem. Commun.*, 2017, **53**, 6520–6523.
31 H. Xu, H. Xu, S. Ma, X. Chen, L. Huang, J. Chen, F. Gao, R. Wang, K. Lou and W. Wang, *J. Am. Chem. Soc.*, 2018, **140**, 16408–16412.
32 S.-P. Han, D.-X. Zhou, P. Lin, Z. Qin, L. An, L.-R. Zheng and L. Lei, *Environ. Toxicol.*, 2015, **30**, 323–331.
33 H. Liu, Y. Sun, Z. Li, J. Yang, A. A. Aryee, L. Qu, D. Du and Y. Lin, *Nanoscale*, 2019, **11**, 8458–8463.
34 S. Cai, C. Liu, J. Gong, S. He, L. Zhao and X. Zeng, *Spectrochim. Acta, Part A*, 2021, **245**, 118949.
35 H. Y. Ahn, K. E. Fairfull-Smith, B. J. Morrow, V. Lussini, B. Kim, M. V. Bondar, S. E. Bottle and K. D. Belfield, *J. Am. Chem. Soc.*, 2012, **134**, 4721–4730.
36 H. Yu, Y. Xiao and L. Jin, *J. Am. Chem. Soc.*, 2012, **134**, 17486–17489.
37 J.-B. Li, Q.-Q. Wang, L. Yuan, Y.-X. Wu, X.-X. Hu, X.-B. Zhang and W. Tan, *Analyst*, 2016, **141**, 3395–3402.
38 M. Dong, Y.-W. Wang and Y. Peng, *Org. Lett.*, 2010, **12**, 5310–5313.
39 E. B. Veale, D. O. Frimannsson, M. Lawler and T. Gunnlaugsson, *Org. Lett.*, 2009, **11**, 4040–4043.
40 Z. Xie, J. Ge, H. Zhang, T. Bai, S. He, J. Ling, H. Sun and Q. Zhu, *Sens. Actuators, B*, 2017, **241**, 1050–1056.
41 T. Cao, D. Gong, S. C. Han, A. Iqbal, J. Qian, W. Liu, W. Qin and H. Guo, *Talanta*, 2018, **189**, 274–280.
42 L. He, X. Yang, Y. Liu, X. Kong and W. Lin, *Chem. Commun.*, 2016, **52**, 4029–4032.
43 J. Xu, Y. Zhang, L. Zeng, J. Liu, J. M. Kinsella and R. Sheng, *Talanta*, 2016, **160**, 645–652.
44 Z. Li, Y. Xu, H. Zhu and Y. Qian, *Chem. Sci.*, 2017, **8**, 5616–5621.
45 L. He, X. Yang, M. Ren, X. Kong, Y. Liu and W. Lin, *Chem. Commun.*, 2016, **52**, 9582–9585.
46 C. Liu, X. Jiao, S. He, L. Zhao and X. Zeng, *Dyes Pigm.*, 2017, **138**, 23–29.